AN APPROXIMATE METHOD OF DIVERGENCE MEASUREMENT

By George P. Cressman

Air Weather Service

(Manuscript received 6 October 1953)

ABSTRACT

With the vorticity equation for horizontal motion as a beginning, and with the aid of several assumptions, the equation $\nabla_H \cdot \boldsymbol{v} = \boldsymbol{v}_T \cdot \nabla_H \ln \eta$ is derived, giving the horizontal divergence as the product of ($\boldsymbol{v}_T$) the vector wind-difference between the level in question and 600 mb, and the logarithm of the absolute vorticity (η) at the level where the divergence is desired. The divergence at 850 mb is computed for a variety of situations with the above equation and is compared with vertical velocities, with the divergence computed from the wind field, and with observed weather distributions, the comparisons yielding favorable results. Finally, suggestions are made for the use of the method for divergence determination in the prognostic routine.

1. Introduction

Numerous studies have been made with the objective of obtaining the weather distribution which would correspond to a given set of prognostic charts for various levels. The most promising line of attack has involved determination of the divergence by means of the vorticity equation, as has been done by Sutcliffe [10] and by Riehl *et al* [9]. This paper will present a simplified method for obtaining divergence, which should be particularly applicable to prognostic charts as well as to current charts.

2. The divergence measurement

The vorticity equation can be written in the form, with reference to horizontal motion,

$$(\boldsymbol{v} - \boldsymbol{c}) \cdot \nabla_H \ln \eta = - \nabla_H \cdot \boldsymbol{v}, \qquad (1)$$

where η is the absolute vorticity about the vertical, $\boldsymbol{v}$ the horizontal wind vector, and $\boldsymbol{c}$ is the horizontal movement in an arbitrary direction of the lines of absolute vorticity. Horizontal solenoids, friction, vertical transport of vorticity, and rotation of vorticity from about a horizontal to about a vertical axis have been neglected.

For the purposes of this development, the existence of a continuous surface of non-divergence in mid-troposphere will be assumed. The vorticity equation written for this level gives

$$(\boldsymbol{v}' - \boldsymbol{c}') \cdot \nabla_H \ln \eta' = 0, \qquad (2)$$

where the primes refer to the surface of non-divergence.

The writer [2] has shown that the lines of absolute vorticity at the various levels have approximately the same orientation. Also, the short-wave troughs and ridges which are identifiable with vorticity maxima and minima move at about the same speed at all levels. $\boldsymbol{c}$ will therefore be assumed equal to $\boldsymbol{c}'$, and the lines of η will be assumed to have the same orientation as the lines of η'. Then one can replace $\boldsymbol{c}$ by $\boldsymbol{c}'$, and then by $\boldsymbol{v}'$, which gives the result that

$$\boldsymbol{v}_T \cdot \nabla_H \ln \eta = \nabla_H \cdot \boldsymbol{v}, \qquad (3)$$

where $\boldsymbol{v}_T = \boldsymbol{v}' - \boldsymbol{v}$, the vector wind-difference between the surface of non-divergence and the surface in question.

In practice, (3) can be applied most easily when the vorticity is approximated by the geostrophic vorticity, and the vertical shear is approximated by the thermal wind. Although the "surface of non-divergence" is really neither continuous nor level, the writer [2] found, in agreement with many previous studies, that (2) is satisfied, in the mean, at about 600 mb. $\boldsymbol{v}_T$ will therefore be represented by the geostrophic-wind difference between the surface where the divergence is desired and 600 mb.

3. Relation of (3) to Sutcliffe's results

From Sutcliffe's work [10], the expression for the relative divergence between two pressure levels may be applied to a surface of non-divergence and some surface below, and written as

$$\nabla_p \cdot \boldsymbol{v}' - \nabla_p \cdot \boldsymbol{v} = - f^{-1} \boldsymbol{v}_T \cdot \nabla_p (\zeta + \zeta' + f), \qquad (4)$$

where f is the Coriolis parameter, and ζ and ζ' are the relative vorticities at the two surfaces. The primes have the same meaning as above. For comparison with (3), (4) can be put in the form

$$\nabla_p \cdot \boldsymbol{v} = f^{-1} \boldsymbol{v}_T \cdot \nabla_p (\eta + \zeta'). \qquad (5)$$

The difference between the form $\nabla \ln \eta$ in (3) and the form $f^{-1} \nabla \eta$ in (5) arises from Sutcliffe's approximation of η by f on the right-hand side of his vorticity equation. A second difference is that ζ' appears in (5) but not in (3). To test the significance of this difference, computations were made on two widely diverse

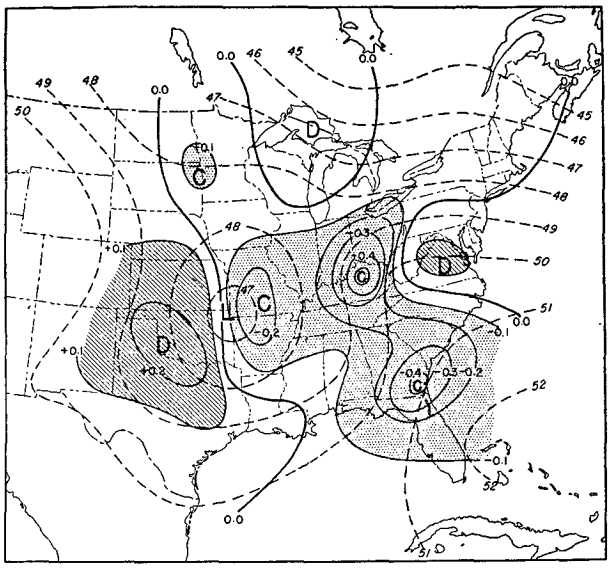

FIG. 1. Computed divergence (10^{-4} sec^{-1}) at 850 mb, 1600 GCT 18 December 1945. Broken lines are 850-mb contours.

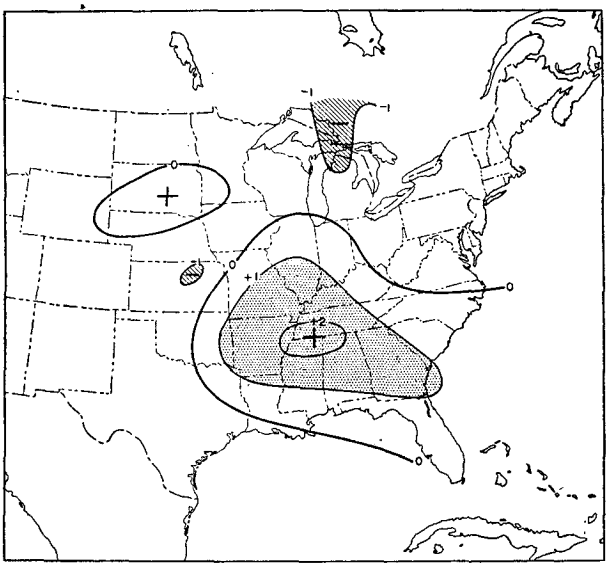

FIG. 2. 24-hr average vertical motion (cm/sec) at 700 mb, centered on 1600 GCT 18 December 1945. (From New York University.)

situations, using the 850- and 600-mb surfaces, of the products $v_T \cdot \nabla_p \ln \eta$ and $v_T \cdot \nabla_p \ln \eta'$. The results (not reproduced here) indicated that the second product is much smaller than the first and is in phase with it (maxima coinciding with maxima, and minima with minima). This leads to the conclusion that the low- (and mid-) tropospheric thermal wind tends to blow along the vorticity lines at 600 mb (and also 500 mb), a fact which has been noted earlier in the preparation of 500-mb vorticity charts. In fact, there is little doubt that a high negative correlation-coefficient exists between temperature and vorticity at 500 mb. This can be used to explain the well-known high correlation between temperature change and pressure change in mid-troposphere.

4. Computation with the divergence equation (3)

The results of an equation such as (3) are difficult to validate by theoretical arguments alone, because of the assumptions made. The best test of divergence charts is comparison with charts of:

1. vertical motion obtained by a different method;
2. divergence obtained by a different method; and
3. weather of various types.

The divergence at 850 mb has been computed from (3) for a number of different synoptic series. The 850-mb surface was selected as a low tropospheric surface at which the assumptions made above should be reasonably well fulfilled. The computations involved the following steps:

1. analysis of the 850-mb chart;
2. computation of the geostrophic absolute vorticity at 850 mb by the method described by the writer [2], and analysis of the vorticity pattern for equal intervals of $\ln \eta$; the grid size used in the geostrophic vorticity computations was 150 nautical miles;
3. preparation of an approximate 600-mb chart by plotting and analyzing for 14,000-ft winds and the average of the heights of the 500- and 700-mb surfaces;
4. superposition of the 850–600-mb thickness pattern on the chart of 850-mb $\ln \eta$, and calculation of the product $v_T \cdot \nabla \ln \eta$.

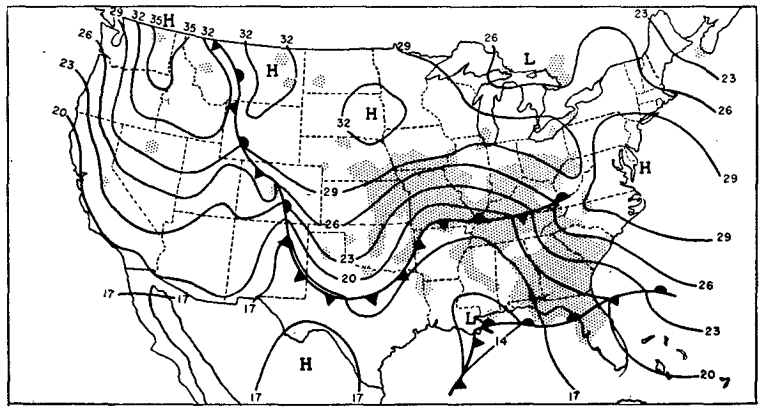

FIG. 3. Surface map for 1830 GCT 18 December 1945. Stipled area indicates precipitation at map time.

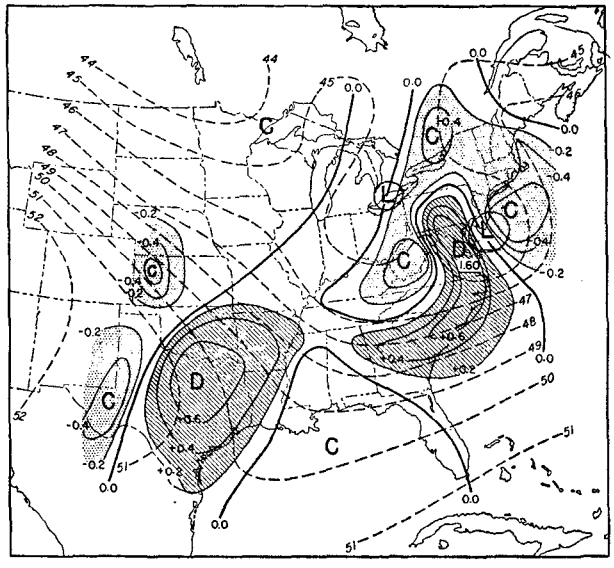

FIG. 4. Computed divergence (10^{-4} sec^{-1}) at 850 mb, 1600 GCT 19 December 1945.

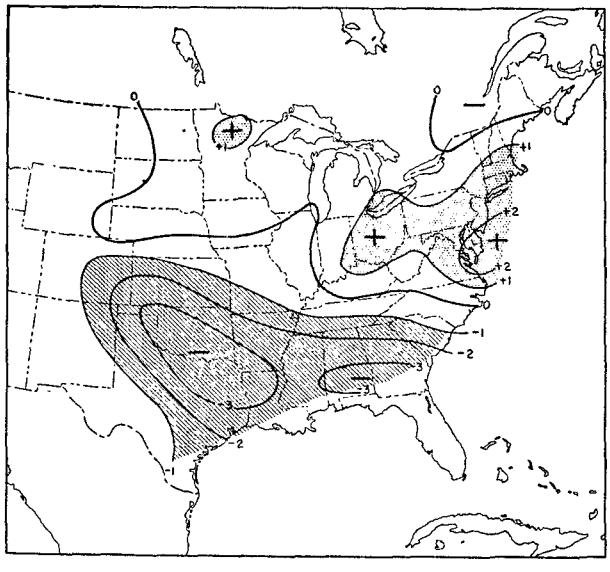

FIG. 5. 24-hr average vertical motion (cm/sec) at 700 mb, centered on 1600 GCT 19 December 1945. (From New York University.)

Several charts were prepared with the 850-mb vorticity computed from a direct analysis of the wind field. This proved to be laborious because of the necessity of preparing streamline and isotach analyses and was abandoned, since the results obtained were only slightly different from those arrived at by the geostrophic approximation. (A different result would probably have been obtained if the computations had been made at higher levels, *e.g.*, 300 mb.)

5. Comparison with charts of vertical motion

A series of charts of vertical motion at 700 mb, computed by the adiabatic method [7] was computed at New York University in 1946. These have been made available by Prof. James E. Miller. Divergence charts at 850 mb were computed from (3) for 1600 GCT on 18 and 19 December 1945. The vertical-motion charts had been computed as 12-hr average motions, centered on the times 1000 and 2200 GCT. The vertical motion charts for these two times were therefore averaged, giving 24-hr average vertical motions centered on 1600 GCT, on both 18 and 19 December 1945. In addition to the vertical-motion charts, the surface weather-maps for 1830 GCT for these two days have been copied from the *Daily weather map* published by the U. S. Weather Bureau.

The 850-mb divergence chart, for 18 December 1945, fig. 1, shows the principal centers of convergence to be over Georgia, Kentucky and Missouri, with a divergence area over Oklahoma and Texas. The accompanying vertical motions, fig. 2, at 700 mb are positive over the convergence area but do not show the detail indicated on fig. 1. Only a small amount of subsidence is shown over the large 850-mb divergence area in the southwest. However, a subsidence area over the Great Lakes corresponds to a weak divergence area indicated at 850 mb. The precipitation pattern on the surface map, fig. 3, shows the same general detail in the southeast as fig. 1, with centers of precipitation over Georgia, Kentucky and Missouri.

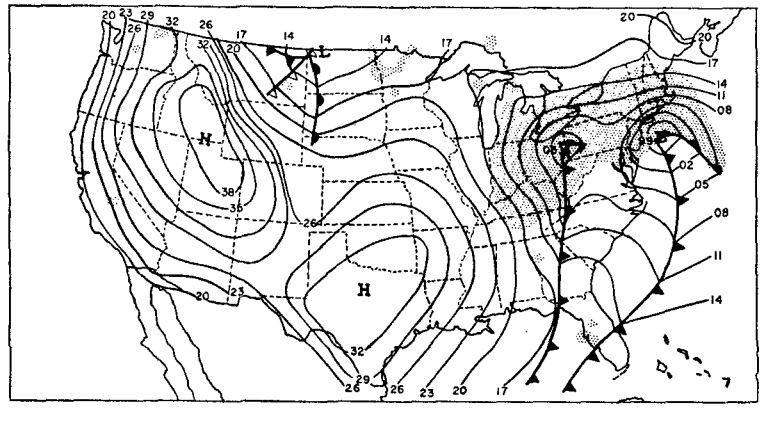

FIG. 6. Surface map for 1830 GCT 19 December 1945. Stipled area indicates precipitation at map time.

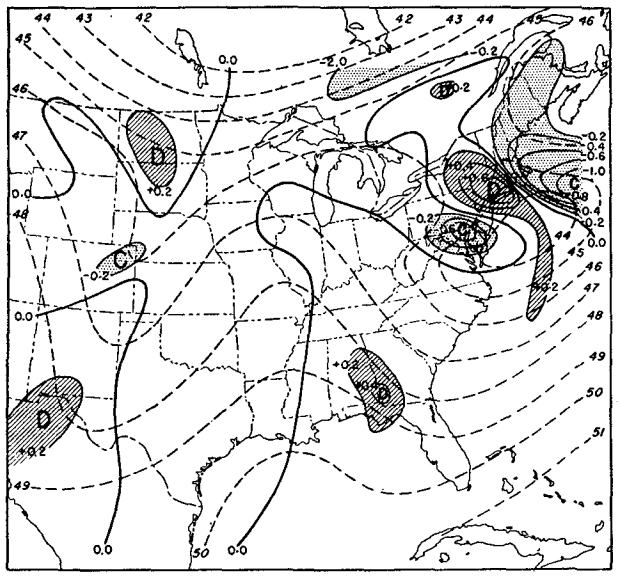

FIG. 7. Divergence (10^{-4} sec^{-1}) computed at 850 mb from (3), 0300 GCT 1 January 1953. Dashed lines are 850-mb contours.

The charts for 19 December 1945 are shown in figs. 4–6. The main area of difference is over Maryland and Virginia, where the very strong divergence computed at 850 mb is not reflected by the vertical motion at 700 mb. This is probably due to the fact that the synoptic pattern was moving rapidly, and a 24-hr average of the vertical motions is considerably smoothed. However, the sea-level chart, fig. 6, shows the divergence to be between two cold fronts, and can be considered as a partial confirmation of the pattern shown in fig. 4. The very high value for divergence would seem entirely unreasonable, unless it is remembered that the whole pattern is rapidly moving. Although very large vertical velocities are suggested, the total vertical displacements of air parcels are not so large, due to this rapid displacement of the patterns.

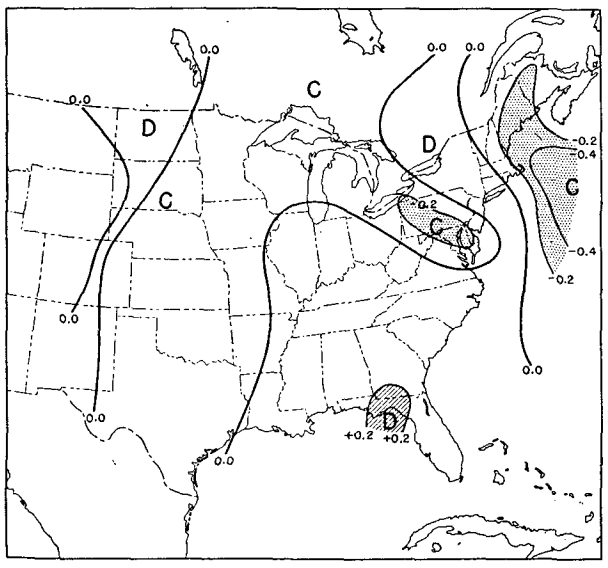

FIG. 8. Divergence (10^{-4} sec^{-1}) computed at 850 mb from wind field, for 0300 GCT 1 January 1953. (From P. Kuhn.)

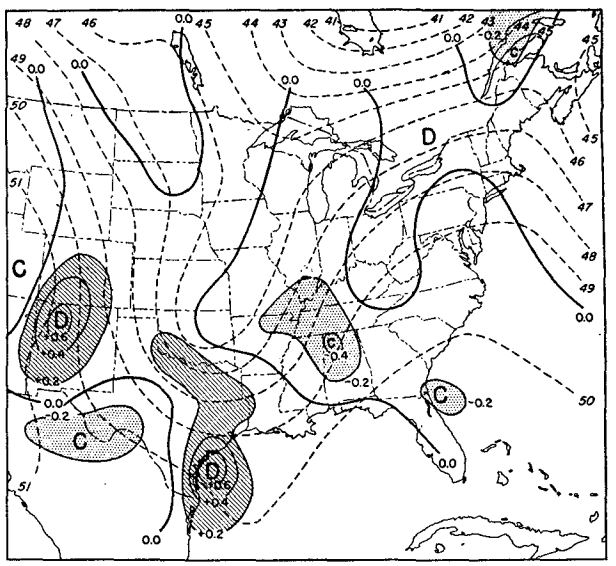

FIG. 9. Same as fig. 7, but for 0300 GCT 2 January 1953.

6. Comparison with other methods of computing divergence

In the course of a study of precipitation by the Short Range Forecast Section of the U. S. Weather Bureau, a series of divergence charts was prepared by Mr. P. Kuhn. These were prepared from measurements of the wind field from the corners of overlapping triangles, 280 nautical miles on a side. This large dimension helps circumvent the difficulties due to inaccurate or unrepresentative wind reports, but results in divergence patterns which are more smoothed than those obtained from the application of (3) with the grid size of 150 nautical miles. Mr. Kuhn has made his charts of divergence at 850 mb available for comparison.

Figs. 7 to 16 show divergence charts computed from (3) and divergence charts computed from the wind field for the first five days in January 1953. With the

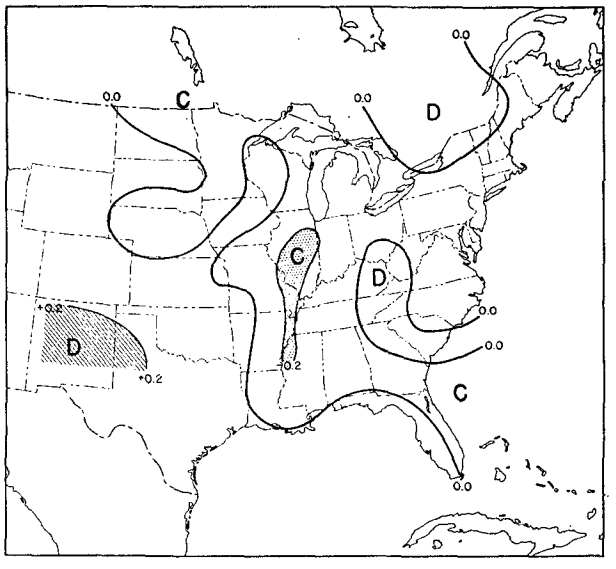

FIG. 10. Same as fig. 8, but for 0300 GCT 2 January 1953.

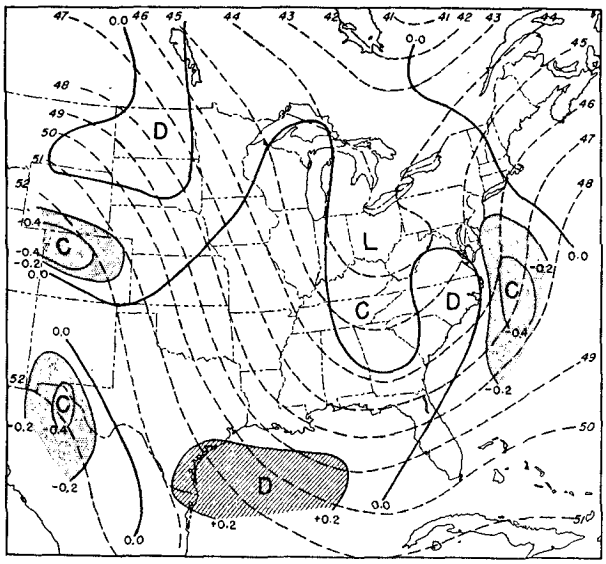

FIG. 11. Same as fig. 7, but for 0300 GCT 3 January 1953.

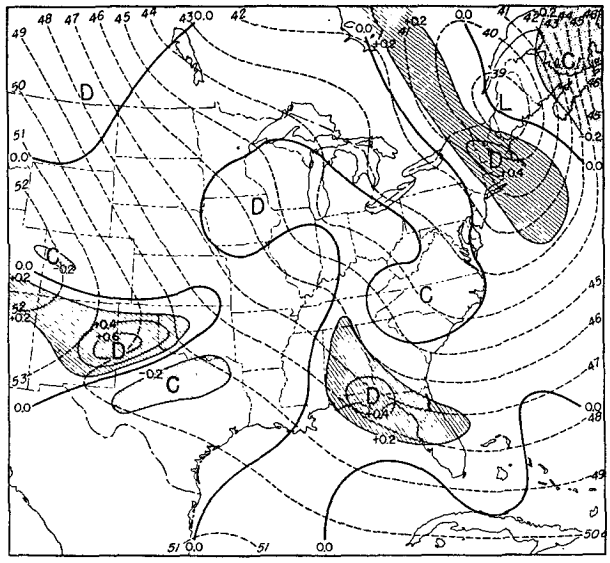

FIG. 13. Same as fig. 7, but for 0300 GCT 4 January 1953.

exception of 2 January, the charts are very similar, the main difference being that the areas of convergence and divergence computed from (3) have higher central values than those computed from the winds, as could be expected from the difference in grid sizes used. The effects of smoothing are particularly evident in the northeast states in figs. 7 and 8, where the strong divergence area over New York in fig. 7 appears much weaker on fig. 8. This is due to its small lateral extent (less than the side of the triangle used in the wind computations), and the convergence areas on each side.

The most important difference between figs. 9 and 10 is in the location of the convergence area in the Mississippi Valley. From the cloud and weather data, it was not possible to determine which one of the two charts is more accurate. In figs. 11 and 12, and figs. 13 and 14, the charts obtained by the two methods are extremely similar. In figs. 15 and 16, there is a slight difference in the location of the convergence area in the southeast.

The good agreement between the divergence charts computed by the two entirely different methods is certainly better than had been expected from the results published by Priestley [8], and indicates that both methods gave reasonably accurate results.

7. Comparison of the divergence charts with the weather

Several charts are presented to show the divergence at 850 mb at times of some interesting occurrences of severe weather. The purpose in presenting these is not so much to explain the weather as to see whether the divergence charts look reasonable.

The first chart of this series, fig. 17, is the 850-mb divergence for 2100 GCT 8 June 1953, the date of

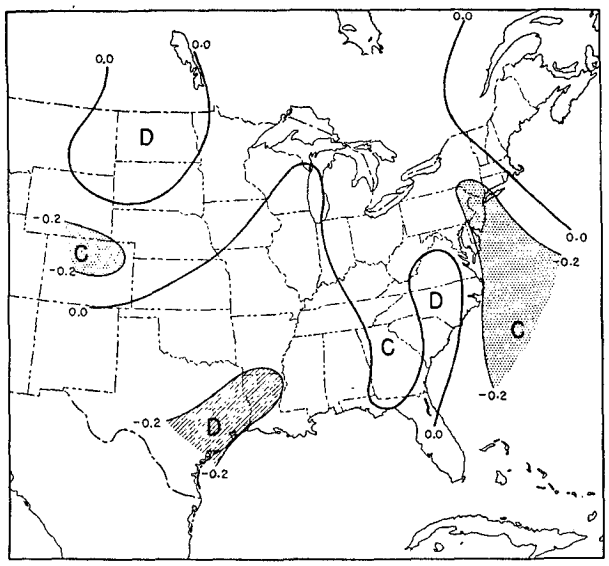

FIG. 12. Same as fig. 8, but for 0300 GCT 3 January 1953.

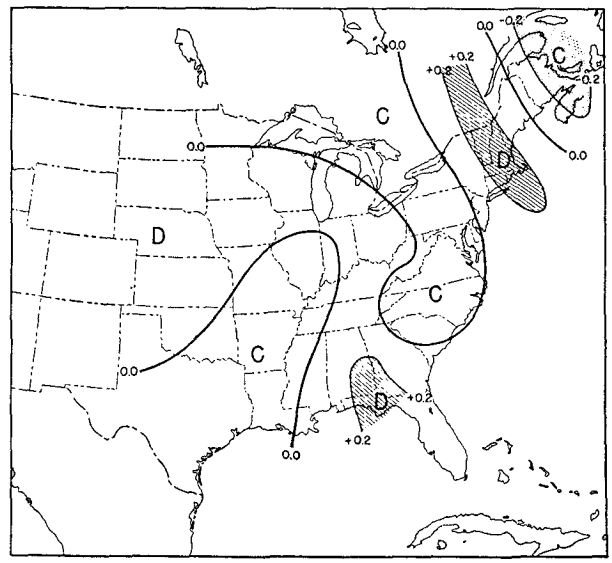

FIG. 14. Same as fig. 8, but for 0300 GCT 4 January 1953.

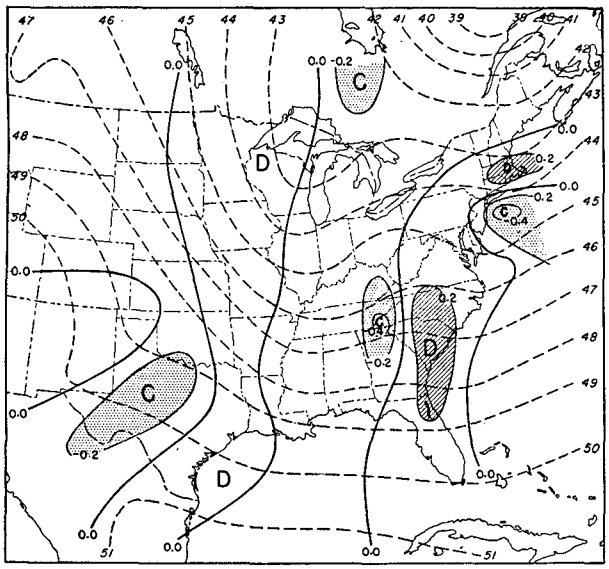

FIG. 15. Same as fig. 7, but for 0300 GCT 5 January 1953.

the tornadoes which caused the great damage and high casualties in Flint, Michigan, and nearby areas. This chart was obtained by linear interpolation, by a graphical method, from the divergence charts for 1500 GCT 8 June and 0300 GCT 9 June. The comparison shows that the tornadoes occurred along a line of maximum convergence. The center of maximum convergence was located farther north, where warm-front rain and maximum pressure falls were found. The convergence at the site of the tornadoes was only 10^{-5} sec^{-1}, a relatively small value compared to some convergences which can be seen on the other figures. This, however, is to be understood as being on a synoptic scale, *i.e.*, detectable from observations spaced several hundred miles apart. The extreme convergences which are associated with individual severe thunderstorms and tornadoes occur on a much smaller scale, and are not detectable by ordinary

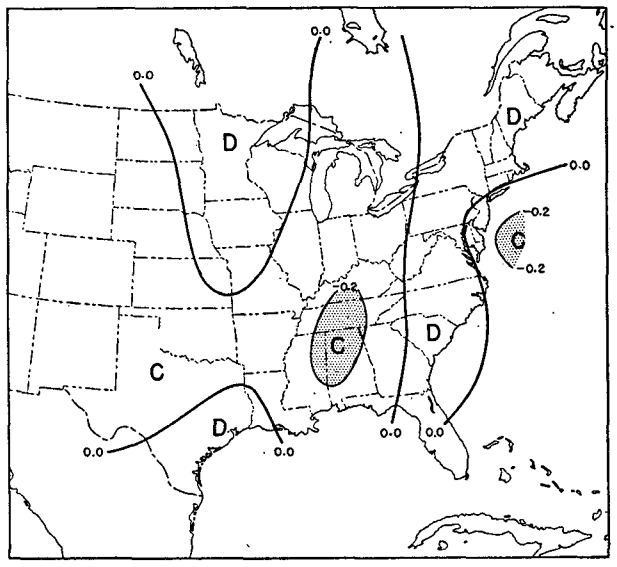

FIG. 16. Same as fig. 8, but for 0300 GCT 5 January 1953.

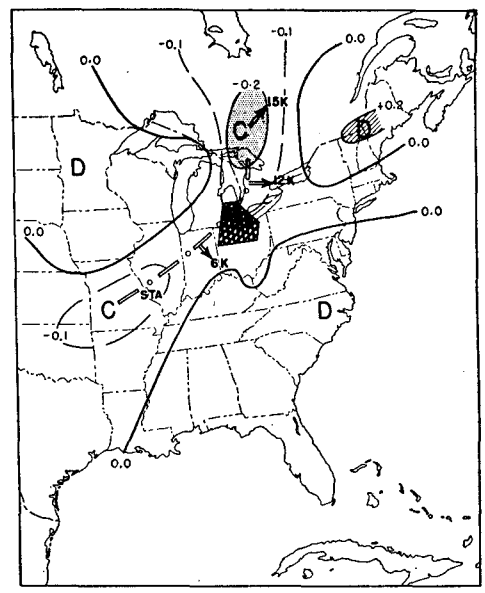

FIG. 17. Computed divergence (10^{-4} sec^{-1}) at 850 mb, 2100 GCT 8 June 1953. Line of maximum convergence is indicated by dot-dashed line, with arrows indicating its movement in knots at map time. Tornadoes occurred in cross-hatched area from 2330 GCT 8 June to 0400 GCT 9 June.

upper-air observing networks. One should not expect the maximum convergence on a large horizontal scale at the site of the tornadoes, since a large amount of convergence would be associated with significant horizontal temperature gradients and would also result in saturation at middle and high levels. Such conditions are not favorable for tornado development (see, for example, Fawbush and Miller [3]).

The situation 24 hr later, at the time of the Worcester, Massachusetts, tornado, is shown in fig. 18. This chart, obtained by the same method as fig. 17, also shows a line of maximum convergence associated with the tornado development. Again, the center of maximum convergence is found farther north, in association with warm-front rain and maximum pressure falls.

It is well known that convergence is a necessary, but

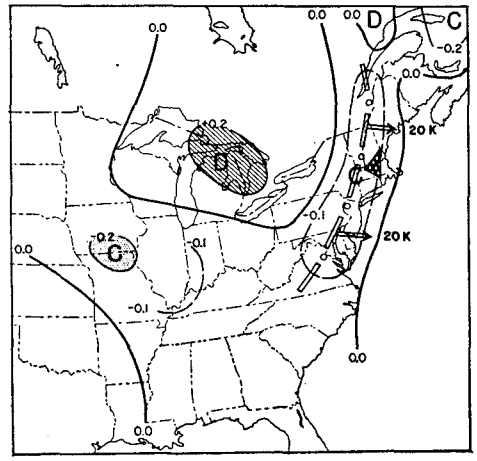

FIG. 18. Same as fig. 17, but for 2100 GCT 9 June 1953. Tornadoes occurred in cross-hatched area from 2030 to 2230 GCT.

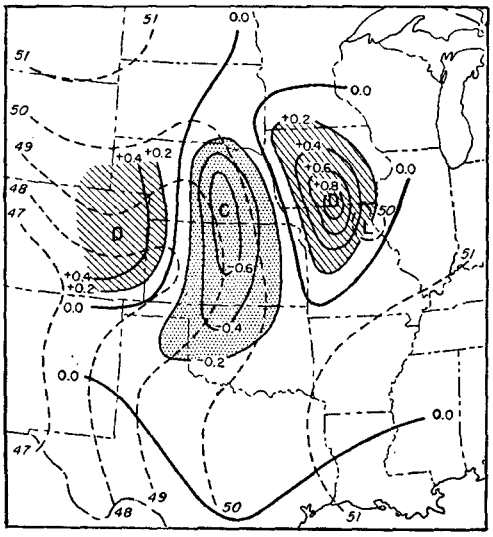

FIG. 19. Computed divergence (10^{-4} sec^{-1}) at 850 mb, 0300 GCT 11 July 1951.

not a sufficient, condition for tornado development. Also, as pointed out above, strong convergence on a large horizontal scale is probably not as effective for producing tornadoes as weaker convergence. The charts shown in figs. 17 and 18, therefore, give patterns agreeable with the tornado development, and seem approximately correct.

The final charts presented are at the time of the heavy rains which led to the Kansas City flood of July 1951. In fig. 19, a convergence center is shown over Kansas and Nebraska, with a central value of nearly 0.8×10^{-4} sec^{-1}, with a divergence center on either side. This convergence center remained about stationary for the following 24 hr.

Approximate rainfall rates (see Fulks[5]) computed from the divergence chart can be used to give a rough check on the magnitude of the computed convergence over Kansas. The precipitation rate was obtained by assuming a linear variation of convergence with pressure, and setting the convergence equal to zero at 600 mb. The sounding used was the Dodge City, Kansas, sounding, after having been lifted to saturation.

The results shown in fig. 20 are to be compared with the observed precipitation shown in fig. 21. Aside from any deficiencies in (3) and its application here, the following difficulties contribute to differences between the two charts:

1. The data density does not permit comparisons on a scale which is a fraction of the distance between upper-air reporting stations; for example, in fig. 20, the 2-in line encloses only one radiosonde- and one wind-observation; no upper-air data at all exist within the 4-in line;
2. None of the 0300 GCT soundings in this area showed any extensive saturation; the Dodge City sounding required an average of 50- or 60-mb lift before saturation was reached; the Oklahoma City and Fort Leavenworth soundings required even more lifting;
3. Instantaneous precipitation rates are calculated, and 24-hr total rainfall is used for verification; fortunately for the comparison, this was a persistent pattern;
4. Other features neglected, but which may influence the results, are the convergence in the friction layer and non-linear variation of convergence with pressure.

With the above in mind, the calculation is seen to be about the right magnitude and centered correctly, indicating acceptable accuracy in the divergence chart.

8. Conclusions

The comparisons made above show that (3) permits a fairly accurate representation of divergence to be made from synoptic charts with the aid of the geostrophic approximation. The quantities used in the measurement are those which can be obtained from prognostic methods. For example, although 850-mb prognostic charts are seldom made, nearly all large forecast-centers prepare prognostic charts for sea

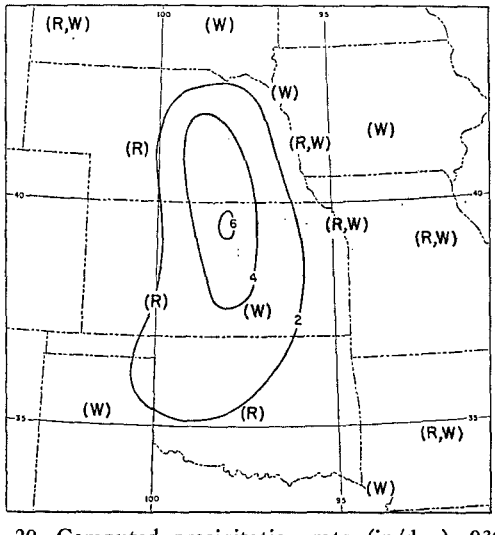

FIG. 20. Computed precipitation rate (in/day), 0300 GCT 11 July 1951. Data distribution at map time is indicated by R for radiosonde report and W for wind report.

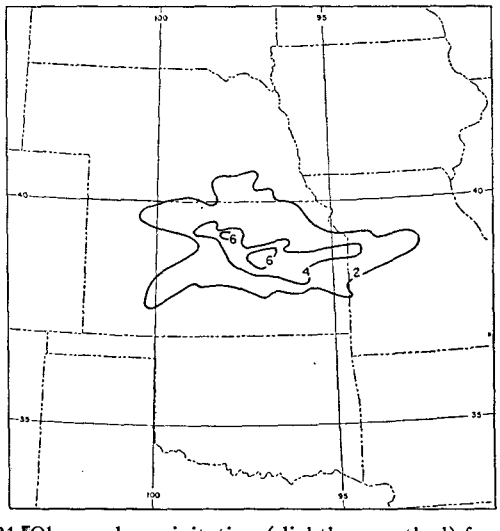

FIG. 21. Observed precipitation (slightly smoothed) from 1830 GCT 10 July 1951 to 1830 GCT 11 July 1951. (From U. S. Weather Bureau [10].)

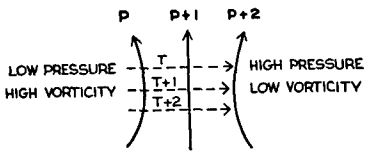

FIG. 22. Hypothetical situation at a low level. Solid lines are isobars; dashed lines are isotherms.

level. They also prepare (or at least should prepare) prognostic charts of the thickness from 1000 to 700 or 500 mb, either directly or in the course of a thickness check. Any given set of such prognostic charts will correspond to a unique solution for the corresponding pattern of sea-level or 1000-mb divergence, which is closely related to vertical motions and weather. A suggested method for the solution is given below:

1. Prepare a chart of the prognostic sea-level vorticity pattern from the sea-level prognostic chart, by calculations at grid points or by the graphical method of Fjørtoft [4]; suitable interpolation can be made to obtain lines spaced at equal intervals of $\ln \eta$;

2. Superimpose on the prognostic vorticity chart the prognostic thickness from 1000 to 700 or 500 mb; the actual magnitude of the divergence is of little importance for daily operational use; the sign and relative magnitude should be sufficient;

3. The vorticity advection need not be computed; it is inversely proportional to the size of the areas formed by intersections of thickness lines with vorticity lines, and can be noted visually.

Actually, after one has obtained some experience in this process, the approximate location and relative magnitude of the divergence patterns can be seen by superimposing the thickness chart on the surface chart. The locations of maximum and minimum vorticity can be noted visually, and the results used qualitatively. Thus, if the thermal wind, as given by the thickness lines, blows from low to high vorticity at the lower level, divergence exists, and *vice versa*.

Equation (3) shows that, insofar as high vorticity is correlated with low pressure and low vorticity correlated with high pressure, divergence is correlated with cold-air advection and convergence with warm-air advection (below 600 mb). The occurrence of warm-air advection in connection with general rainfall [11], thunderstorms [6], and other severe weather has long been recognized. This correlation is also related to the high negative correlation between advective and non-advective thickness changes in the lower half of the troposphere [1].

The approximate relation between advection and divergence is illustrated in fig. 22. In the hypothetical low-level situation, low pressure and high vorticity are found together, as are high pressure and low vorticity, giving warm-air advection together with convergence [from (3)]. Cold-air advection with divergence can be seen if one reverses the direction and labels of the isotherms. It is not to be supposed that the negative correlation between pressure and vorticity is consistently high, but fig. 22 shows what happens when it is high.

Due to the assumptions made in its development, (3) is of course not suitable for divergence measurements in mid troposphere or for detailed examinations of the variation of divergence with height. It does, however, seem to give a satisfactory one-parameter picture of divergence and vertical motion, and due to its uncomplicated nature can, if desired, be used to simplify the temperature equation in the "$2\frac{1}{2}$-dimensional" numerical prediction model.

Acknowledgments.—The writer wishes to thank Mr. P. Kuhn for making his divergence charts available for comparison, Dr. C. Gilman for suggesting the analysis of the July 1951 storm, and Prof. J. E. Miller for making the New York University vertical-motion charts available.

REFERENCES

1. Craddock, J. M., 1951: Advective temperature change in the 1,000–700 mb and 700–500 mb layers. *Quart. J. r. meteor. Soc.*, **77**, 51–60.
2. Cressman, G. P., 1953: An application of absolute vorticity charts. *J. Meteor.*, **10**, 17–24.
3. Fawbush, E. J., and R. C. Miller, 1952: The mean tornado sounding. *Bull. Amer. meteor. Soc.*, **33**, 303–307.
4. Fjørtoft, R., 1952: On a numerical method of integrating the barotropic vorticity equation. *Tellus*, **4**, 179–194.
5. Fulks, J. R., 1935: Rate of precipitation from adiabatically ascending air. *Mon. Wea. Rev.*, **63**, 291–294.
6. Means, L. L., 1944: The nocturnal maximum occurrence of thunderstorms in the midwestern states. *Dept. Meteor. Univ. Chicago, Misc. Rep.*, No. 16, 38 pp.
7. Panofsky, H. A., 1946: Methods of computing vertical motion in the atmosphere. *J. Meteor.*, **3**, 45–49.
8. Priestley, C. H. B., 1949: An experiment on the analysis of horizontal divergence. *Wea. Devel. Res. Bull., Commonwealth Austral.*, No. 14, 22–29.
9. Riehl, H., K. Norquest and R. Sugg, 1952: A quantitative method for the prediction of rainfall patterns. *J. Meteor.*, **9**, 291–298.
10. Sutcliffe, R. C., 1947: A contribution to the problem of development. *Quart. J. r. meteor. Soc.*, **73**, 370–383.
11. U. S. Weather Bureau, 1952: Kansas-Missouri floods of June–July 1951. *Tech. Pap.*, No. 17, 105 pp.